Bloch Equation in the Rotating Frame, Multidimensional Excitation

John M. Pauly
Magnetic Resonance Systems Research Laboratory,
Stanford University

Highlights This talk will describe the design of selective excitation pulses in one and multiple dimensions. The viewer will learn about:

- Small-tip-angle excitation with Fourier transform designs in one and multiple dimensions
- Large-tip-angle design of 1D Pulses
- Adiabatic pulses
- Multidimensional pulses combining all of these elements
- Spectral-spatial pulses that are selective in frequency and space

Introduction One of the most important tools for MRI is the ability to selectively manipulate the magnetization with radio frequency (RF) pulses. These can provide selectivity in space, frequency, and relaxation times T_1 and T_2. This presentation outlines the basic ideas behind RF pulses, describes the types of operations RF pulses can perform, and then goes through the various different types of RF pulses and pulse design methods. The goal is to give an overview of what RF pulses can do, and where to look for more information. A good reference for all of these topics is ref. [1].

Fourier Transform Designs The concept of k-space and the Fourier transform apply to excitation, just as they do to imaging The Bloch equation without relaxation is ,

$$\frac{d\mathbf{M}}{dt} = \gamma \begin{pmatrix} 0 & \mathbf{G}(t)\cdot\mathbf{x} & -B_{1,y}(t) \\ -\mathbf{G}(t)\cdot\mathbf{x} & 0 & B_{1,x}(t) \\ B_{1,y}(t) & -B_{1,x}(t) & 0 \end{pmatrix} \mathbf{M} \tag{1}$$

where $B_1(t)$ is the complex RF, and $\mathbf{G}(t)$ is the gradient vector. If the initial magnetization is aligned with the $+z$ axis and the RF flip angle is small, the transverse magnetization M_{xy} after an RF pulse of duration T is given by

$$M_{xy}(\mathbf{x}, T) = iM_0 \int_0^T \gamma B_1(t) e^{i\mathbf{k}(t)\cdot\mathbf{x}} dt \tag{2}$$

where $\mathbf{k}(t)$ is a spatial frequency variable given by the integral of the remaining gradient area

$$\mathbf{k}(t) = -\gamma \int_t^T \mathbf{G}(s) ds. \tag{3}$$

The transverse magnetization is the transform of the applied RF energy along a k-space trajectory determined by the gradient waveform.

Fig. 1 shows simple interpretation in 1 D. If we assume that the RF waveform is partitioned into small segments that each act independently, each segment produces a small amount of transverse magnetization. This magnetization precesses under the effect of the applied gradient, and accrues a phase proportional to the integral of the remaining gradient. The total magnetization is the integral of the contributions of all of these small segments of RF.

For a constant gradient, the slice profile is the transform of the RF waveform, Fig. 2. The RF waveform (left) is chosen such that its frequency spectrum excites a well defined slice (right). This is a Hamming windowed sinc waveform, commonly used as an excitation pulse.

A useful concept for selective excitation is the "time-bandwidth product," TBW, which is duration of the pulse multiplied by width of the passband. Pulses with the same time-bandwidth product have the same shape, even if they have different durations. The example in Fig. 2 has a time-bandwidth product of 8. Typically this is the num-

Proc. Intl. Soc. Mag. Reson. Med. 23 (2015)

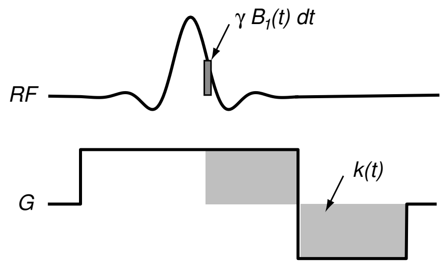

Figure 1: Small-excitation approximation. Each increment of the RF, $\gamma B_1(t)dt$, produces transverse magnetization. This precesses under the influence of the remaining gradient. The integrated remaining gradient is $\mathbf{k}(t)$, so the accumulated phase shift is $e^{i\mathbf{k}(t)\cdot\mathbf{x}}$. The slice profile expression in Eq. 2 integrates over the entire waveform.

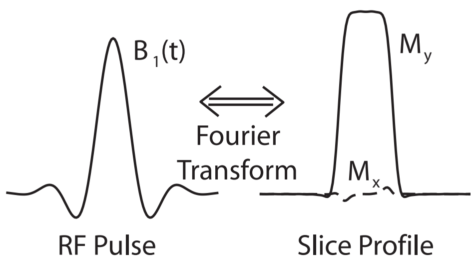

Figure 2: A small-excitation RF pulse (left) and slice profile (right).

ber of zero crossings of the RF waveform, which is also 8 for this example. With a $TBW = 8$, a 4 ms pulse has a bandwidth of $8/4 = 2$ kHz. With a 1 G/cm gradient, or 4.257 kHz/cm, this is a little less than a 5 mm slice.

Large Flip Angle Pulses RF pulses designed using linear Fourier transform designs work poorly for large-flip-angle inversion and spin-echo pulses. However, we can represent the desired rotation by two complex coefficients, called spinor representation. The Shinnar-Le Roux (SLR) transform invertably relates the RF pulse to the magnetization profile. We can then use the Fourier transform to design the spinor slice profiles, and the inverse SLR transform to solve for the corresponding RF pulse. Hence, the small-tip-angle design methods, plus the inverse SLR transform, allow the exact design of large-flip-angle pulses.

Spinors Methods based on calculating the final magnetization produce by an RF pulse are are limited, since this is insufficient to fully characterize the rotation produced by the pulse. A more convenient approach uses the spinor representation of rotations, which only requires two complex numbers to completely characterize the rotation. Given the spinor, the effect of the RF pulse on any initial magnetization can be calculated.

The Bloch equation in the absence of relaxation reduces to a sequence of rotations. Although we can solve for these rotations by multiplying 3x3 matrices, there is a much simpler representation using 2x2 complex matrices and spinors. A rotation by an angle ϕ about an axis $\mathbf{n} = (n_x, n_y, n_z)^T$ is represented by the matrix

$$Q = \begin{pmatrix} \alpha & -\beta^* \\ \beta & \alpha^* \end{pmatrix} \tag{4}$$

where

$$\alpha = \cos(\phi/2) - i\, n_z \sin(\phi/2) \tag{5}$$

$$\beta = -i\,(n_x + i\, n_y)\sin(\phi/2). \tag{6}$$

These satisfy the constraint

$$\alpha\alpha^* + \beta\beta^* = 1. \tag{7}$$

Note that the rotation angle appears as a half-angle in Eq. 6. The effect of a sequence of rotations is computed by multiplying out the 2x2 complex matrices. Note that the matrix is completely determined by the first column $(\alpha, \beta)^T$, so that a pair of complex numbers is all that is needed to represent a rotation.

Once the rotation produced by an RF pulse has been computed, we would like to know what effect it has given some initial magnetization. For an excitation pulse, given an initial magnetization along $+z$, the result is

$$M_{xy}^+ = 2\alpha^*\beta M_0. \tag{8}$$

For an inversion or saturation pulse, the initial magnetization is the same, but we are concerned with the longitudinal magnetization. This is given by

$$M_z^+ = (1 - 2\beta\beta^*)M_0. \tag{9}$$

Spin-echo pulses produce two terms, the spin echo and the unrefocused magnetization which is usually suppressed with dephasing gradients. If we assume the initial magnetization is along $+y$, the spin-echo component is

$$M_{xy}^+ = i\,\beta^2 M_0. \tag{10}$$

Given α, β, and the initial magnetization, it is very easy to compute the final magnetization for most types of RF pulses.

The Shinnar-Le Roux Algorithm Remarkably, given a representation of a slice profile in an appropriate form, it is also easy to solve for the RF pulse that will produce it. The Shinnar-Le Roux Algorithm approximates a continuous RF pulse as a sequence of impulsive RF pulses interspersed with free precession intervals. It results in the spinor representation of the slice profile to be given by $A_N(z)$ and $B_N(z)$, two N^{th} order polynomials in $z = e^{i\gamma Gx\Delta t}$ where Δt is the sampling time.

The significance of this representation is that it is invertible. This inversion procedure can be used to design RF pulses by designing the $A_N(z)$ and $B_N(z)$. The two polynomials must satisfy the amplitude constraints implicit in Eqs. 6 and 7. From Eq. 6 the function $B_N(z)$ should be chosen to approximate the sine of half the desired rotation angle, with a constant phase determined by the desired rotation axis. The magnitude of $A_N(z)$ is determined by the magnitude constraint Eq. 7. A minimum power solution uniquely determines $A_N(z)$. Once $A_N(z)$ has been computed, the two polynomials are processed using the inversion procedure to produce the RF waveform. This design procedure is the Shinnar-Le Roux algorithm.

An example of this method is shown in Fig. 3, which demonstrates the design of a spin-echo pulse. We start by choosing a $B_N(z)$ that approximates the desired profile. This can be just about any function that could be used as a lowpass digital filter. In this example we use the same Hamming windowed sinc for Fig. 2, which is sometimes itself used as a spin-echo pulse. From Eq. 6 $B_N(z)$ must be scaled so that the passband has an amplitude of $\sin\phi/2 = \sin\pi/2 = 1$. This is plotted in Fig. 3. The $A_N(z)$ polynomial is then computed by the magnitude constraint, Eq. 6, and the minimum power criteria. The RF pulse is then computed using the SLR inversion procedure. The resulting RF pulse and spin-echo profile are also shown in Fig. 3c and d.

Although this procedure may appear complex, it is actually very simple. The slice profile is determined by $B_N(z)$, which is designed as RF pulses themselves have traditionally been designed, using

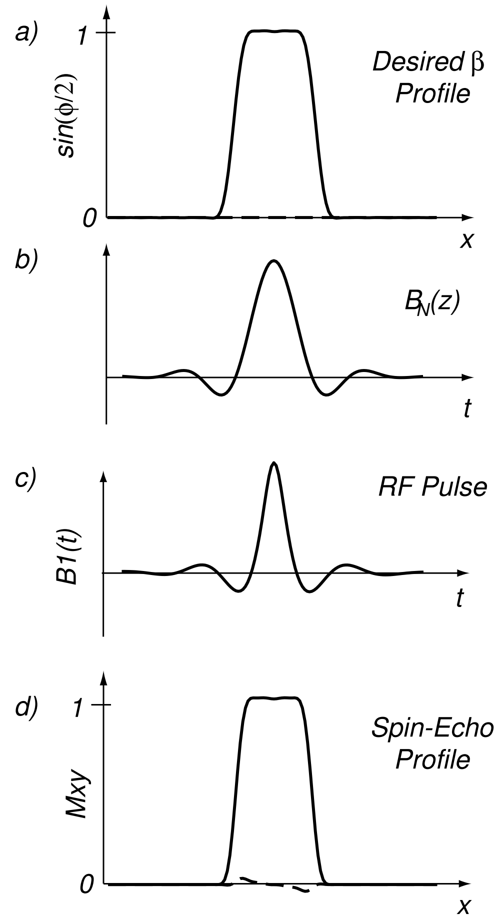

Figure 3: Illustration of the design process in the SLR algorithm. In (a) the profile of $B_N(z)$ is chosen and scaled to produce the right flip angle. The transform of this profile is the $B_N(z)$ polynomial (b). The inverse SLR transform $\mathcal{SLR}^{-1}(B_N(z))$ produces the spin-echo RF pulse (c). The profile of the refocused magnetization is shown in (d).

Fourier transform arguments. The flip angle is determined by the scaling of $B_N(z)$. The rest of the procedure is deterministic, and can be considered a black box. For convince, we'll denote this black box as the "inverse SLR transform",

$$B_1(t) = \mathcal{SLR}^{-1}(B_N(z)). \tag{11}$$

One Dimensional Pulses A wide variety of types of RF pulses can be designed by using different initial $B_N(z)$ polynomials. The main considerations are what the pulse will be used for, and whether the slice profile phase can be exploited.

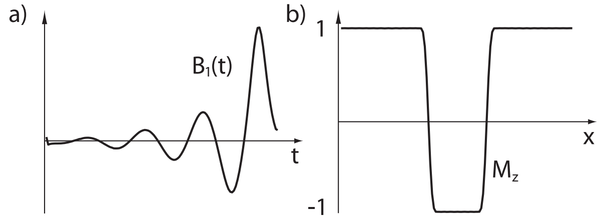

Figure 4: Minimum-phase inversion pulse (left) and inversion profile (right).

Linear-Phase Pulses Slice-selective excitation pulses and spin-echo pulses have maximum signal if the phase across the slice is linear. A linear-phase excitation pulse is perfectly refocused with a gradient reversal. A linear-phase RF pulse is produced by starting with a linear phase $B_N(z)$. These are hermitian symmetric about the midpoint, as in Fig. 3.

There are two costs for linear phase. One is that a linear-phase pulse also maximizes the peak RF power. Another is that the slice profile is not as selective as minimum/maximum phase or non-linear phase pulses can be.

Minimum/Maximum-Phase Pulses For other types of pulses, the phase of the profile is not an issue. This is true of inversion pulses and saturation pulses, where any transverse magnetization is generally suppressed with a dephasing gradient. In this case, we can improve the selectivity of the profile by starting with a minimum or maximum phase design. This can be almost twice as selective as a linear-phase pulse for the same duration.

A minimum phase pulse has most of the RF energy at the end of the pulse. A maximum-phase pulse is a minimum-phase pulse played in reverse order. An example of a minimum-phase inversion pulse is shown in Fig. 4.

Nonlinear-Phase Pulses While minimum and maximum phase pulses have sharper slice profiles than linear-phase pulses, they require very close to the same peak power. Peak power is often the primary practical concern when designing pulses. Lower peak power can often be obtained by using a non-linear phase RF pulse. These can be designed by starting with a minimum phase $B_N(z)$. If this has a time-bandwidth product of M, there

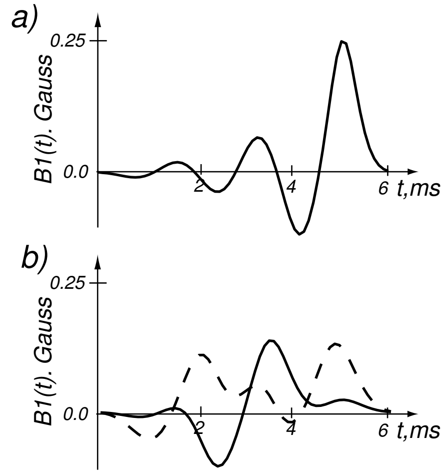

Figure 5: Comparison of a minimum phase and an optimized non-linear phase inversion pulses. Both pulses have identical inversion profiles. The optimized non-linear phase pulse has 56% of the amplitude of the minimum phase pulse, or 31% of the peak power. The integrated power of the two pulses is identical.

are 2^M possible phase profiles that have an identical magnitude profile. These can be searched to optimize a particular parameter, such as peak RF power. An example of an inversion pulse designed with this approach is shown in Fig. 5, along with the minimum phase pulse with the identical profile. In this case the peak amplitude has been reduced to 56%. Note that the integrated power remains the same. The use of non-linear phase simply distributes this power more uniformly along the length of the pulse.

For higher time-bandwidth pulses, exhaustive searches become impractical. A preferred approach is to choose a target quadratic phase profile, and construct $B_N(z)$ so as to closely approximate this profile. This is the approach used by Le Roux in the design of his Very Selective Saturation (VSS) pulses [2].

Adiabatic Pulses Another class of non-linear phase RF pulses are adiabatic pulses, which are designed from a completely different perspective. The idea here is that the frequency and amplitude of the RF pulse are smoothly swept, to keep the magnetization either aligned with or orthogonal to the effective RF vector. The most important example is the hyperbolic secant pulse, shown in Fig. 6. An

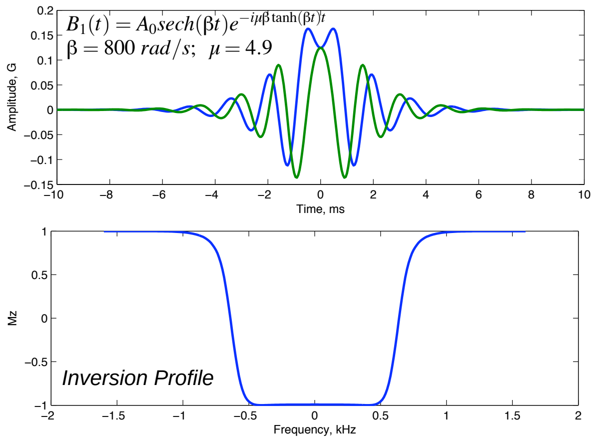

Figure 6: A hyperbolic secant RF pulse (top) and it's inversion profile (bottom). The hyperbolic secant is an adiabatic pulse, that produces a high fidelity inversion profile for any RF level above a given threshold.

adiabatic pulse performs an inversion for any RF level above a given threshold. These are very useful when accurate inversions are required, or when the homogeneity of the RF field is inadequate. Using combinations of half sweeps, adiabatic pulses can be designed for any flip angle [1]. Adiabatic pulses can be optimized for a wide range of operating conditions by optimizing the envelope and sweep rate, and by starting with an SLR pulse and adding a frequency sweep [3,4].

Multidimensional Selective Excitation RF pulses that are selective in multiple dimensions can also be designed. In the small-tip-angle case Fourier transform arguments can be used, and the result is directly analogous to the image reconstruction problem for an arbitrary k-space trajectory. For the large-tip-angle case, the issues are more complex. Fourier transform designs can still be used if certain symmetry requirements are met. However, the important case of large-flip-angle spectral-spatial pulses is a non-linear problem.

Fourier Transform Multidimensional Pulses For non-constant gradients and in multiple dimensions the k-space velocity should be normalized

$$M_{xy}(\mathbf{x}, T) = iM_0 \int_0^T \frac{\gamma B_1(t)}{|\gamma \mathbf{G}(t)|} e^{i\mathbf{k}(t)\cdot\mathbf{x}} |\gamma \mathbf{G}(t)| dt. \tag{12}$$

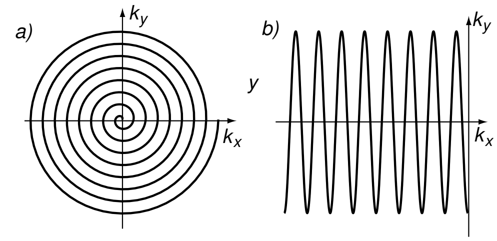

Figure 7: A spiral k-space trajectory (a) and an EPI trajectory (b). As a direct parallel to the imaging case, either of these can be used as the basis of a 2D RF pulse. Many other trajectories are also possible.

The $\mathbf{G}(t)$ is chosen to trace out a pattern that uniformly covers a region of k-space. Two common examples are shown in Fig. 7. As in imaging, the rate at which this pattern is traced out varies due to the limitations of the gradient system hardware. As a result, the RF waveform that should be applied is the sampled transform of the desired profile, compensated by the k-space velocity. An additional compensation term is required if the k-space trajectory is non-uniform [5,6], just as in imaging.

The excited volume can be shifted to any position $\mathbf{x_0}$ by modulating the RF waveform with $e^{-i\mathbf{k}(t)\cdot\mathbf{x}_0}$. Effectively, this keeps the point $\mathbf{x}_0$ exactly on resonance as the gradient waveform is played out.

An example multidimensional RF pulse is shown in Fig. 8. This is a 2D selective excitation pulse based on a spiral gradient. The gradient spirals in to the center so that no refocusing lobe is required. This pulse excites a cylinder, limited in $x - y$ plane, and extending in z.

This type of pulse is often used to restrict excitation to a single column or "pencil" to allow tracking of very rapid motion, such as in MR m-mode [7], or for navigator acquisitions [8].

Echo-Planar and Spectral-Spatial Pulses Non-linear multidimensional pulses can be designed by using the SLR algorithm in one dimension, and linear designs in the remaining dimensions. This is the approach for pulses based on the EPI trajectory, Fig. 7. This can be used as the basis of a 2D spatial excitation RF pulse, and can be used for limiting the FOV for fast imaging. A recent example is restricted FOV diffusion imaging [9].

EPI design are also the basis for spectral-spatial pulses [10] which is simultaneously selective in

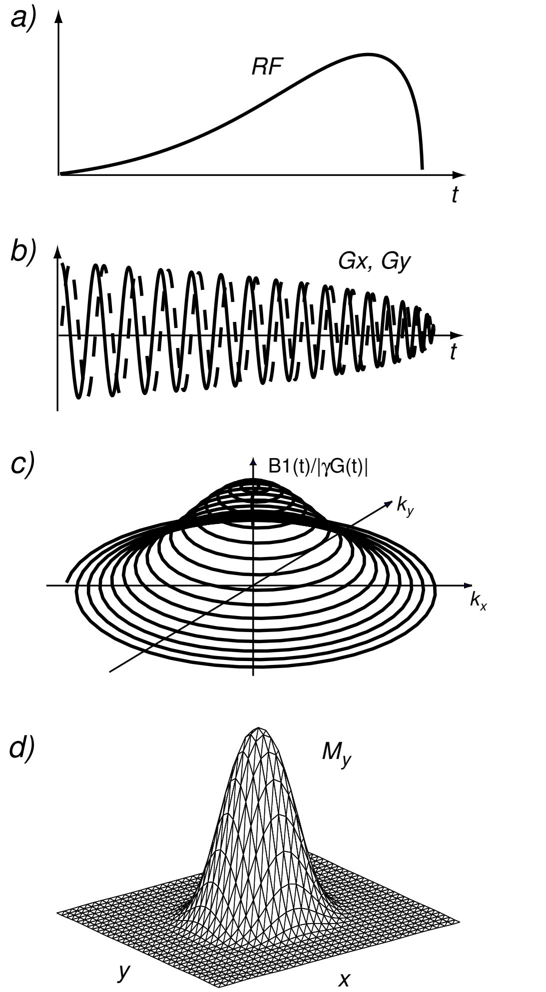

Figure 8: 2D RF pulse (a), gradients (b), k-space weighting (c), and excitation profile (d).

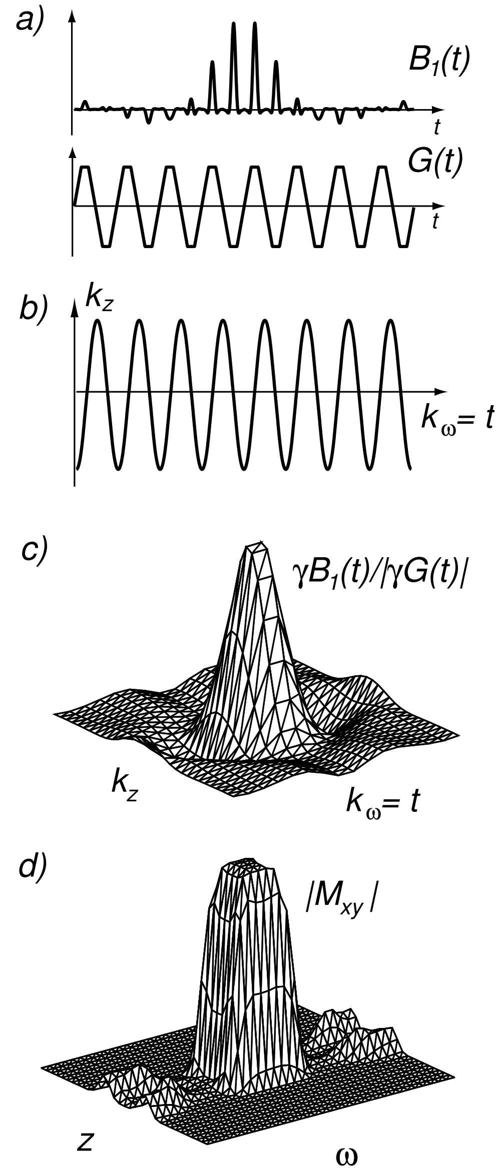

Figure 9: Spectral-Spatial spin-echo RF pulse and gradient, k-space trajectory (b), k-space weighting (c), and spin-echo profile (d).

both space and frequency. Spectral-spatial pulses are used for lipid suppression for fast EPI or spiral imaging, where lipids would otherwise produce image artifacts [11]. They are also usefull for spectroscopic imaging for water suppression [12] or individually exciting combinations of resonances in hyperpolarized ^{13}C MRSI [13].

A spectral-spatial pulse is based on a conventional echo-planar k-space trajectory. For a 2D spatial pulse the constant gradient in the "phase-encode" direction establishes a linear distribution of frequencies, and the RF pulse selects a range of these frequencies. For a spectral-spatial pulse, we use the same RF pulse, but eliminate the constant gradient. This leaves us with a pulse that is frequency selective as well as spatially selective.

While spectral-spatial pulses can be designed using the small-excitation approximation, as in Fig. 8, this approach degrades as the flip angle increases. For spin-echo or inversion pulses, the nonlinearity of the Bloch equation must be considered. An effective approach is to use an SLR design in the spectral dimension, and the small-rotation approximation in the spatial domain [14]. Spin-echo pulses designed with this approach can produce excellent water suppression for MRSI experiments [12]. Figure 9 is a spin-echo pulse designed with this approach. By replacing the 1D subpulses with 2D spirals, a 3D pulse, or a 2D spatial, 1D spectral pulse can also be produced [15].

Spectral-spatial pulses have some interesting properties. They don't exhibit displacement with frequency offset. The spectral-spatial pulse spatial profile is only perfect exactly on resonance, but this point can be shifted in the design to improve performance at any particular frequency. This is useful for improving the depth of a stopband [14] or eliminating an N/2 sidelobe [16].

The spectral dimension can also be designed using a sampled adiabatic pulse, or a self-refocused pulse [17]. Two such pulses can be used in a PRESS MRSI pulse sequence, with the spatial selectivity on different axes, to provide both spatial localization and excellent water suppression [12].

References

[1] M. Bernstein, K. King, and J. Zhou. *Handbook of MRI Pulse Sequences*. Elsevier Press, 2004.

[2] P. Le Roux, R. J. Gilles, G. C. McKinnon, and P. G. Carlier. Optimized outer volume suppression for single-shot fast spin-echo cardiac imaging. *J Magn Reson Imaging*, 8(5):1022–32, 1998.

[3] P. Balchandani, J. Pauly, and D. Spielman. Slice-selective tunable-flip adiabatic low peak-power excitation pulse. *Magn Reson Med*, 59(5):1072–1078, May 2008.

[4] P. Balchandani, J. Pauly, and D. Spielman. Designing adiabatic radio frequency pulses using the Shinnar-Le Roux algorithm. *Magn Reson Med*, 64(3):843–851, Sep 2010.

[5] C.J. Hardy, H.E. Cline, and P.A. Bottomley. Correcting for nonuniform *k*-space sampling in two-dimensional NMR selective excitation. *J. Magn. Reson.*, 87:639–645, 1990.

[6] C. J. Hardy and P. A. Bottomley. 31P spectroscopic localization using pinwheel NMR excitation pulses. *Magn Reson Med*, 17(2):315–27, 1991.

[7] H. E. Cline, C. J. Hardy, and J. D. Pearlman. Fast MR cardiac profiling with two-dimensional selective pulses. *Magn Reson Med*, 17(2):390–401, 1991.

[8] Y.L. Liu, S.J. Riederer, P.J. Rossman, R.C. Grim, J.P. Debbins, and R.L. Ehman. A monitoring, feedback, and triggering system for reproducible breath-hold MR imaging. *Magn. Reson. Med.*, 30(4):507–11, 1993.

[9] E. U. Saritas, C. H. Cunningham, J. H. Lee, E. T. Han, and D. G. Nishimura. DWI of the spinal cord with reduced FOV single-shot EPI. *Magn Reson Med*, 60(2):468–473, Aug 2008.

[10] C. H. Meyer, J. M. Pauly, A. Macovski, and D. G. Nishimura. Simultaneous spatial and spectral selective excitation. *Magn Reson Med*, 15(2):287–304, 1990.

[11] C.H. Meyer, B.S. Hu, D.G. Nishimura, and A. Macovski. Fast spiral coronary artery imaging. *Magn. Reson. Med.*, 28(2):202–213, December 1992.

[12] J. Star-Lack, D. B. Vigneron, J. Pauly, J. Kurhanewicz, and S. J. Nelson. Improved solvent suppression and increased spatial excitation bandwidths for three-dimensional PRESS CSI using phase-compensating spectral/spatial spin-echo pulses. *J Magn Reson Imaging*, 7(4):745–57, 1997.

[13] P. E. Larson, R. Bok, A. B. Kerr, M. Lustig, S. Hu, A. P. Chen, S. J. Nelson, J. M. Pauly, J. Kurhanewicz, and D. B. Vigneron. Investigation of tumor hyperpolarized [1-13C]-pyruvate dynamics using time-resolved multiband RF excitation echo-planar MRSI. *Magn Reson Med*, 63(3):582–591, Mar 2010.

[14] J. Pauly, D. Spielman, and A. Macovski. Echo-planar spin-echo and inversion pulses. *Magn Reson Med*, 29(6):776–82, 1993.

[15] J. M. Pauly, B. S. Hu, S. J. Wang, D. G. Nishimura, and A. Macovski. A three-dimensional spin-echo or inversion pulse. *Magn Reson Med*, 29(1):2–6, 1993.

[16] Y. Zur. Design of improved spectral-spatial pulses for routine clinical use. *Magn Reson Med*, 43(3):410–20, 2000.

[17] P. Balchandani, M. Yamada, J. Pauly, P. Yang, and D. Spielman. Self-refocused spatial-spectral pulse for positive contrast imaging of cells labeled with SPIO nanoparticles. *Magn Reson Med*, 62(1):183–192, Jul 2009.